Cell Viability and Probe-Cell Membrane Interactions of XR1 Glial Cells Imaged by Atomic Force Microscopy

Scott S. Schaus and Eric R. Henderson
Signal Transduction Training Group, Department of Zoology and Genetics, Iowa State University, Ames, Iowa 50011 USA

ABSTRACT As atomic force microscopy (AFM) imaging of live specimens becomes more commonplace, at least two important questions arise: 1) do live specimens remain viable during and after AFM, and 2) is there transfer of membrane components from the cell to the AFM probe during probe-membrane interactions? We imaged live XR1 glial cells in culture by single- or dual-pass contact or tapping-mode AFM, examined cell viability at various postimaging times, and report that AFM-imaged live XR1 cells remained viable up to 48 h postimaging and that cell death rates did not increase. To determine if nonlethal, transient interactions between the AFM probe and cell membrane led to transfer of XR1 cell membrane phospholipid components on the probe, we treated the scanned probes with the lipid-binding fluorophore FM 1-43. Confocal microscopy revealed that phospholipid membrane components did accumulate on the probe, and to a generally greater extent during contact-mode imaging than during tapping-mode imaging. Moreover, membrane accumulations on the probe were greater when live XR1 cells were damaged or perturbed, yet membrane did not accumulate in fluorescently detectable quantities during repeated "force curves" during control experiments. Taken together, our data indicate that although AFM imaging of live cells in culture does not affect long-term cell viability, there are substantial probe-membrane interactions that lead to transfer of membrane components to the probe.

INTRODUCTION

In the decade after the first report of the atomic force microscope (AFM) (Binnig et al., 1986), great excitement has surrounded its biological applications, especially to living specimens. Topographic data and submicron resolution from the AFM provide advantages over traditional light microscopy techniques and have led to novel images of live specimens, of varied subcellular structures and components, and of biological processes in living cells. Examples of such AFM images include, but are not limited to cell surface morphology (Barbee et al., 1994, 1995; Beckmann et al., 1994; Hoh and Schoenenberger, 1994; Hörber et al., 1992; Kasas et al., 1993; Oberleithner et al., 1994), the cytoskeleton and cytoskeletal elements (Braunstein and Spudich, 1994; Chang et al., 1993; Henderson et al., 1992; Lal et al., 1995; Parpura et al., 1993), cell migration and locomotion (Fritz et al., 1994; Oberleithner et al., 1993), organelles and organelle movement (Braunstein and Spudich, 1994; Fritz et al., 1994; Schoenenberger and Hoh, 1994), platelet activation (Fritz et al., 1994), cell volume (Schwab et al., 1995), micromechanical changes in cell membranes (Hoh and Schoenenberger, 1994; Shroff et al., 1995), viral budding (Häberle et al., 1992), secretory structures (Schneider et al., 1997; Spudich and Braunstein, 1995), neuron differentiation (Bonfiglio et al., 1995), and neurite outgrowth (Lal et al., 1995).

During AFM imaging, a sharp stylus (tip) is scanned in an x-y raster pattern over the sample, and a feedback control circuit adjusts the stylus in the z axis to maintain either a constant vertical applied force (constant force mode), a constant height (constant height mode), or constant amplitude damping (tapping mode). The stylus may have continuous, intermittent, or no direct contact with the specimen surface during imaging (contact, tapping, and noncontact modes, respectively), and, to date, all interpretable images of living cellular specimens have been acquired in either the continuous or intermittent contact modes. Because there is direct contact between the stylus and the specimen surface(s) in these modes, understanding the effects of probe-specimen surface interactions on specimen viability is of primary importance for AFM imaging of living biological specimens.

Recently, many groups have begun to elucidate the biophysical and biomechanical interactions between the stylus and phospholipid membranes in both whole-cell and artificial membrane systems (Hörper et al., 1995; Putman et al., 1994; Radmacher et al., 1995; Raedler et al., 1995; Ricci and Grattarola, 1994; Shroff et al., 1995; Tao et al., 1992), yet there have been only two reports of specific cell viability assays (trypan blue exclusion; Le Grimellec et al., 1994; Schneider et al., 1997). However, AFM imaging of living cells has been conducted over relatively long periods of time (up to 44 h; Hoh and Schoenenberger, 1994), with accompanying morphological and physiological evidences of cell viability and normal functioning, including lamellipodial advancement and retraction, neurite outgrowth, organelle movements, and platelet activation (referenced above).

Previous research in our laboratory (Henderson et al., 1992) and from the Gaub group (Fritz et al., 1994) has led

Received for publication 15 October 1996 and in final form 2 June 1997.
Address reprint requests to Dr. Eric R. Henderson, Signal Transduction Training Group, Department of Zoology and Genetics, 2112 Molecular Biology Building, Iowa State University, Ames, IA 50011. Tel.: 515-294-2876; Fax: 515-294-0345; E-mail: schaus@iastate.edu or telomere@iastate.edu.

0006-3495/97/09/1205/10 $2.00

to three hypotheses about the interactions between the integrated AFM stylus and cell membranes during AFM imaging of live cells. One postulate states that the vertical applied force (applied load) from the scanned probe stylus causes the membrane to "drape" over the relatively rigid subcellular structures during the imaging process, thus revealing these structures. A second hypothesis asserts that the stylus penetrates the cell membrane and directly contacts subcellular structures during imaging. The entropic repulsion model suggested by Fritz et al. proposes that the entropy elasticity of the cell surface glycocalyx could give rise to a short-range repulsive force between the tip and cell surface, lowering the net force between the tip and membrane and limiting lateral resolution at low imaging forces. The repulsive force could be overcome by increasing the applied load, permitting the tip to contact the cell membrane. Each of these proposed tip-membrane mechanisms could result in transient or permanent damage to the primary selective barrier of the cell, the cell membrane.

Favorable evidence for the "draping" model has recently been provided by Haydon et al. (1996), who report that an intracellularly loaded fluorophore does not escape into the surrounding medium, provided relatively blunt AFM probes and epifluorescence microscopy are used. We elected to take a complementary approach and hypothesize that if the AFM stylus truly disrupts or penetrates the cell membrane, small fluorophores that otherwise would be excluded from the cell may be able to enter the cell by diffusion. Provided these fluorophores are nonfluorescent extracellularly and become fluorescently activated or enhanced intracellularly, epifluorescence microscopy could be used to indirectly detect AFM stylus penetration or disruption of the cell membrane. Even if the cell membrane is disrupted transiently during AFM imaging but is undetectable by our assay, we postulate that the cell membrane suffers no permanent structural or functional damage and thus AFM imaged cells should remain viable in culture. Finally, because the stylus usually contacts the cell membrane during AFM imaging, we predict that membrane components could accumulate on the stylus in fluorescently detectable quantities.

As a first approach to answering these fundamental questions, we used a two-component fluorophore assay to provide evidence that single- and dual-pass scanning in both contact or tapping mode AFM have no deleterious effects on cultured XR1 glial cell viability for up to 48 h postimaging. This viability assay is based on intact biochemical processes required to activate the calcein-AM fluorophore and on the cell membrane-dependent exclusion of the DNA-binding ethidium homodimer-1 fluorophore. Although long-term cell viability was not compromised, we found that cellular lipid-based membrane components do accumulate on the probe during the AFM imaging process, indicating direct physicochemical interactions between the AFM probe and the glial cell membrane. Moreover, our data provide preliminary evidence that tapping-mode imaging is generally less invasive than contact mode, as indicated by qualitatively reduced accumulations of membrane components on the imaging probe.

MATERIALS AND METHODS

XR1 cells

XR1 glial cells (*Xenopus laevis* retinal neuroepithelium) were grown in culture according to the protocol of Sakaguchi (Sakaguchi and Henderson, 1993; Sakaguchi et al., 1989). Confluent cell cultures were harvested by trypsin treatment for 10 min, and the cell suspensions were centrifuged at 2800 × *g* for 10 min. After the supernatant was discarded, the pellet was resuspended in an appropriate volume of culture media (60% L15, Sigma, St. Louis, MO; 10% fetal calf serum, Upstate Biotechnology, Lake Placid, NY; *Xenopus* embryo extract) to bring the cell concentration to ~10^6 cells/ml. A 5-μl aliquot of the cell suspension was added to a culture dish (custom made and ECL-treated, see below) containing 700 μl of culture medium. The dish was gently agitated, covered, and incubated at ambient conditions. All experiments were done on cultures 18–24 h after plating.

Culture dish preparation

Custom culture dishes were needed to observe cells simultaneously with coaxial AFM and light microscopy. Briefly, a centered, 25-mm hole was cut into the bottom of a standard 60-mm polystyrene culture dish (09-753-52A; Fisher), and a detergent-washed, Dasag glass coverslip (no. 1.5, 30-mm round; Fisher) was bonded to the underside of the dish by a continuous bead of Sylgard 182 (ET033384; Dow-Corning) deposited around the perimeter of the centered hole. Overnight incubation at 60°C cured the Sylgard and formed a watertight seal between the dish and the glass coverslip. The resulting built-in basin facilitated cell washing as well as media containment during AFM scanning, and the thin glass coverslip permitted examination of the cells by transmitted light and epifluorescence microscopy with high-magnification, short-working-distance objectives.

Before cells were plated in the custom-made culture dishes, two additional preparations were carried out. First, two or three 50-mesh EM locator grids were glued to the bottom of the glass coverslip with Formvar (4% v:v in 1 N 1,2- dichloroethane). Second, to facilitate cell spreading and growth, the culture surface of the glass coverslip was treated with ECL (entactin, collagen IV, laminin; Upstate Biotechnology; 50 μg/ml in 60% L15) and incubated overnight at 4°C. Immediately before a cell suspension aliquot was deposited, the ECL solution was aspirated from the dishes and 700 μl of sterile culture media was added. Unused ECL-treated dishes received 200 μl of sterile phosphate-buffered saline, were stored at 4°C, and were used within 7 days of ECL treatment.

Atomic force microscopy

A NanoScope III BioScope (Digital Instruments, Santa Barbara, CA) equipped with a "G" scanner (106 × 106 × 5 μm, *x, y, z* scan range) was used for all AFM imaging experiments. The BioScope combines features of a standard AFM with those of an inverted optical microscope and thus provides for coaxial observation of the sample (Vesenka et al., 1995). AFM scanning occurred over the nonadherent surfaces ("top") of the specimen, and light microscopy from the adherent side ("bottom") of the specimen was used. During this study epifluorescence microscopy, transmitted light microscopy, and confocal scanning laser microscopy (CSLM) were used; however, epifluorescence microscopy and CSLM were not used simultaneously with AFM during these experiments.

Immediately before AFM imaging, cell cultures were washed three times with 500 μl of sterile 60% L15. In the initial experiments, 350–400 μl of 2× calcein-AM and 350–400 μl of 2× ethidium homodimer-1 were added as the imaging medium. Unfortunately, the calcein fluorophore of the LIVE/DEAD assay (see below) caused deleterious photodynamic effects; thus the protocol was modified so that imaging occurred in either 1) 750-1000 μl of sterile 60% L15 buffer only, or 2) 750-1000 μl of 1×

ethidium homodimer-1 in 60% L15. Suitable XR1 cells (flat, adherent, >50 μm diameter, and within the EM grid locator) were identified with light microscopy and the location was recorded. Cells were scanned with 200-μm long, 20-μm leg-width Si_3N_4 "V" probes (nominal spring constant k = 0.06 N/m) (Digital Instruments). Probes exhibiting a reflected laser sum of less than 3.5 V or a geometrically nonuniform reflected laser spot were rejected (D'Costa and Hoh, 1995). The probe was engaged in a 100 × 100 nm scan area over a cell-free region of the glass substrate, providing a 1:1 coupling ratio between the stylus and the substrate for an accurate calibration of the cantilever sensitivity. For constant force contact mode scanning (CMAFM), force versus distance graphs ("force curves") were obtained, and the piezo control parameters were adjusted to maintain loading forces of ≤1 nN. For tapping mode imaging (TMAFM), the default engagement force provided the most stable images. Integral and proportional gains were held constant across all experiments (2.0 and 4.0 V, respectively). To reduce noise that was particularly dominant in the error signal mode (deflection, amplitude, and phase) data types (Putman et al., 1992), all cell AFM images were acquired while the glass substrate was coupled to a 63× objective (Plan-Apo, NA 1.4; Zeiss, Jena, Germany) via an immersion oil droplet (n_e = 1.518; Zeiss).

After the adjustments to the z piezo parameters, the target cell was moved into the projected scan field with the microscope x-y stage translator so that the stylus was below the cell (with respect to the field of view) for scan up acquisitions, or above the cell for scan down acquisitions. The scan size was successively enlarged from the engagement size (100 nm) to the full-field size (94–100 μm), and the applied force setpoint and z piezo position were adjusted accordingly to maintain initial conditions. For samples scanned at 5 Hz, the loading force and scan parameter adjustments were made at 1 Hz, and the scan rate was then increased to 5 Hz immediately preceding image acquisition.

Single-pass (scan up or scan down) and dual-pass (both scan up and down) AFM images were acquired at 1-Hz or 5-Hz fast scan rates in either contact or tapping mode. All 1-Hz images were 100 × 100 μm scan size, whereas the 5-Hz images were 94 × 94 (TM) or 96 × 96 μm (CM), because of inherent limitations of the piezo at this scan rate. Each image was acquired at 512 samples per line; thus the fast scan direction speed ranges from 100 μm s^{-1} (at 1 Hz) to 480 μm s^{-1} (at 5 Hz), and the slow scan direction speed from 0.2 μm s^{-1} (at 1 Hz) to 0.9 μm s^{-1} (at 5 Hz). Height and deflection data were collected for CM images, and height, amplitude, and phase data were collected for TM images. Images were corrected for warp and bend by a manual planefit (with the glass substrate as a reference), and all height mode images, except where noted, were highpass-filtered to enhance edge contrast.

Immediately after AFM imaging, cells were washed three times with 500 μl of 60% L15, and 1000 μl of cell culture media (60% L15/10% fetal calf serum/1% EE) was added, and the dishes were covered and incubated at ambient conditions.

Cell viability assays

XR1 cells were examined for viability with the LIVE/DEAD *Euko*Light assay (Molecular Probes, Eugene, OR). The LIVE/DEAD assay consisted of two fluorophores, calcein-AM (calcein) and ethidium homodimer-1 (EthD-1). Calcein-AM was membrane-permeant, and upon entry into the cytoplasm the acetoxy-methyl group was cleaved by nonspecific esterases, yielding formaldehyde and the calcein fluorophore, which was visualized with a Zeiss 09 filter set (BP 450–490 nm excitation, FT 510 nm, LP 520 nm emission; hereafter, 488 nm). EthD-1, on the other hand, was excluded from cells that had an intact cell membrane, and only entered cells with damaged or compromised cell membranes. Upon entry into a cell, EthD-1 diffused to the nucleus and intercalated in the minor groove of dsDNA, becoming fluorescently enhanced. EthD-1 was visualized with a Zeiss 15 filter set (BP 546/12 nm excitation, FT 580, LP 590 nm emission; hereafter, 529 nm).

To determine a linear working range of concentrations for the fluorophores, XR1 cell suspensions were distributed in 96-well plates, and methanol (100%) was added to 48 wells to kill cells and provide a positive dead cell assay. The LIVE/DEAD fluorophores were added in a serial dilution series to the wells, and fluorescence was quantified in a microtiter plate reader (FluoroSkan II v3.1; TiterTek). The linear range for both components of the LIVE/DEAD *Euko*Light assay on XR1 glial cells was determined to lie between 1 and 10 μM. For XR1 cells grown in culture dishes, positive controls of cell death were prepared by adding digitonin (50 mM stock,~1 mM final; Sigma) to the culture media, either concurrently with calcein-AM or after the live cell assay was completed.

At 24 or 48 h after AFM imaging, cell cultures were washed three times with 60% L15. Equal volumes (250 μl) of each 2× indicator solution (calcein-AM and EthD-1, both 8 μM, in 60% L15) were added to each culture dish. These preparations were incubated in a dark chamber for 10 min at room temperature, were washed three times with 60% L15, and a final volume of 1000 μl of fresh 60% L15 media was added.

To collect LIVE/DEAD cell viability data, epifluorescence microscopy was done as follows. AFM-imaged cells were located in the EM grid system and examined under four epifluorescence conditions: 1) 25× (total magnification; Zeiss 10× Neo-Fluar), 488-nm filter set exposure, which provided viable cell control data from neighboring non-AFM scanned cells; 2) 25×, 529-nm filter set exposure, which provided nonviable cell control data; 3) 100× (Zeiss 40× Neo-Fluar), 488-nm filter set exposure, for examination of AFM-scanned cell viability; and 4) 100×, 529-nm filter set exposure for examination of AFM-scanned cell death. Photodynamic toxicity was a major issue with the calcein fluorophore, and thus cells were limited to two exposures at 488-nm conditions. Optimal camera back shutter settings (determined from a bracketing series) for Kodak Ektachrome Elite II 400 slide film and Kodak Gold 400 print film were 1–2 s for the 488-nm exposures and 0.25 s for the 529-nm exposures. However, 488-nm filter set exposures were generally acquired in the shutter-priority mode (variable shutter speed, dependent upon the available light) with full-field metered matrix exposure control (Nikon 6006, Tokyo, Japan), because total fluorescence varied from sample to sample. Five control sample dishes were prepared for the LIVE/DEAD assay in the same fashion, but photomicrographs were only acquired at 100×, for both 488-nm and 529-nm filter sets.

Confocal scanning laser microscopy

After each AFM cell imaging session, the probe was transferred to a storage container, and a sufficient volume of 60% L15 was added to cover the entire probe and cantilever substrate. To accurately position the tip for examination by CSLM, the probe was remounted in the AFM fluid cell and placed onto the BioScope scanner. A clean, sterile, custom-made culture dish was placed in the stage sample holder, and 1000 μl of ultrapure H_2O was added to the dish. The probe tip was centered in the field of view, engaged with the glass coverslip at a scan size of 100 × 100 nm, then immediately withdrawn to a distance of ~10–25 μm.

For each probe examined by CSLM (Odyssey; Noran Instruments, Middleton, WI), a confocal reflected image (63×, NA = 1.4, Zeiss Neo-Fluar objective, 217× total magnification, pinhole size 9–10 μm) was first acquired. Next, 5 μl of ice-cold FM 1-43 (1 mM stock, 5 μM final; Molecular Probes, Eugene, OR) was added to the water in the culture dish, and after a 10-min incubation a confocal fluorescence image (488 ± 1.1 nm excitation; 515-nm LP barrier filter, rejection at 488 nm = 4×10^{-4}; 100-μm slit) was acquired from the same focal plane as the reflected image. Because the imaging software uses rectangular pixels rather than square pixels, all CSLM images were aspect ratio corrected with the imaging software (Image-1; Universal Imaging Corporation, West Chester, PA) before transfer to a Macintosh computer for compositing. CSLM images were composited in Photoshop (v 3.0.5; Adobe, Mountain View, CA) as follows. Tonal corrections were applied to raw images, then the images were changed to indexed color mode. A custom gold ramp color look-up table (CLUT) was applied to the reflected images (AFM probe data), whereas a custom green ramp CLUT was applied to the fluorescent images (FM 1-43 data). The images were then changed to RGB mode, and corresponding reflected and fluorescent data were copied to separate layers in a new file and brought into register. The reflected image data were left

in "normal" layer mode, and the fluorescent image data were set to "screen" layer mode at 100% opacity. The composited files were then flattened and saved in TIFF format for output.

Video microscopy

Bright-field videomicroscopy of the AFM imaging of XR1 cells was captured to VHS or S-VHS video (AG-1970 VCR; Panasonic, Seacaucus, NJ) through a color CCD (XC-999; Sony, Tokyo, Japan) attached to the side port of the Axiovert 135 portion of the BioScope. Videos were digitized with a MoviePak Pro Suite (RasterOps, Waco, TX) to a Macintosh 7100/66 PowerPC. Digital video was processed, composited, and output to digital video, analog video, and single frame file series with Premiere (v4.21; Adobe).

RESULTS AND DISCUSSION

AFM imaging and cell viability

We first performed cell viability assays on XR1 cell suspensions with the LIVE/DEAD *Eukol*ight protocol to determine characteristic results of the assays and to determine the linear concentration range for each of the fluorophores. The linear concentration range in XR1 glial cells for both calcein-AM (calcein) and ethidium homodimer-1 (EthD-1) is 1–10 μM (data not shown). We next verified the efficacy of these concentration ranges on XR1 cells grown in the custom-made culture dishes. For positive controls of cell death, XR1 cells in culture were killed by the addition of 50 mM digitonin. Fig. 1, *a–c*, shows a bright-field micrograph of XR1 cells in culture and representative epifluorescence microscopy results of the cell viability assays on XR1 cells in culture. An added value of the "live" assay is that the entire expanse of the cell is visualized because the calcein fluorophore is distributed throughout the cytoplasm and is not quickly compartmentalized, providing complementary morphological data.

AFM imaging of XR1 cells with the BioScope proved abstruse at first, because of the inverted nature of the AFM scanner—with the BioScope AFM the probe, rather than the specimen, is scanned in the *x,y,z* axes. This design permits coaxial observation of the specimen, but in our case—live XR1 cells grown on custom culture dishes—noise artifacts initially masked the authentic error signal data (deflection data in contact mode, amplitude and phase data in tapping mode). Analysis of a Fourier transform of a "noisy" error signal data set revealed that the noise signals were discrete from the sample's true error signal data and could be removed in Fourier space (Fig. 2; also see Fig. 5 *k*). These limitations were readily overcome by coupling the glass coverslip to an oil immersion objective, indicating that this noise was probably generated by sympathetic vibrations of the glass coverslip in the custom-made culture dish.

To determine if the cell membrane was compromised or disrupted during the AFM imaging process, we initially carried out simultaneous AFM and LIVE/DEAD EukoLight assays. If the cell membrane is structurally or physiologically compromised by the AFM scanning process, the EthD-1 fluorophore could enter the cell, diffuse to the nucleus and bind to DNA, and undergo fluorescence enhancement. In the initial protocol, calcein and EthD-1 fluorophores were added to the culture medium immediately before AFM imaging. EthD-1 fluorescence was not detectable during AFM scanning; however, these results must be cautiously interpreted in light of two considerations: 1) EthD-1 fluorescence transmission may have been reduced because of the presence of a 650-nm cutoff filter (Omega Optical, Brattleboro, VT) in the light path to reduce scattered AFM laser light; and 2) the time courses for membrane penetration or disruption by the stylus and for the diffusion constant of EthD-1 may not be comparable. Unfortunately, repeated excitations of the calcein fluorophore caused photodynamic effects that led to blebbing in the XR1 cells, followed by cell death (see Fig. 1 *d*). Further tests on the photodynamic phenomena in XR1 cells established that we were limited to two or three

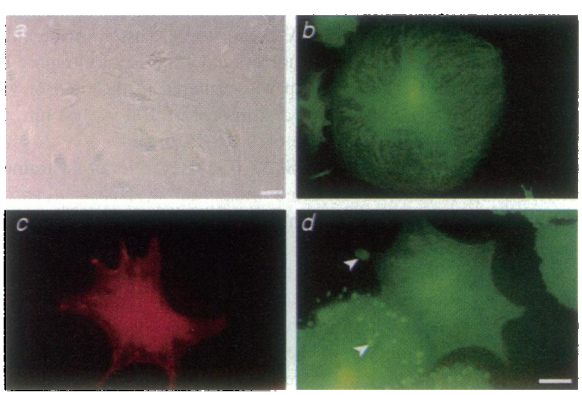

FIGURE 1 XR1 cell characteristics. (*a*) Light micrograph of XR1 cells in culture. (*b,c*) Representative results from LIVE/DEAD EukoLight assay. (*b*) A fluorescence micrograph of XR1 cell viability, evidenced by nonspecific esterase activity required to cleave calcein-AM. Cell margins are visible because of distribution of the fluorophore throughout the cytoplasm. (*c*) Digitonin-induced cell death, indicated by entrance of ethidium homodimer-1 into the cell and subsequent fluorescence enhancement upon binding of DNA. (*d*) Fluorescence micrograph of photodynamic effects and blebbing (*arrowheads*) induced by prolonged exposure to 488-nm excitation. Scale bars = 25 μm.

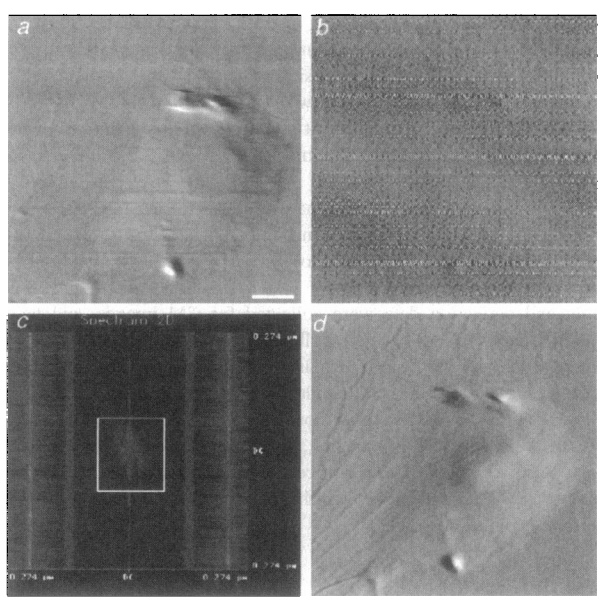

FIGURE 2 Removal of noise artifacts from error signal mode AFM data. (*a*) Highpass-filtered AFM height image of a live XR1 cell with contact-mode AFM at 1.0-Hz fast scan rate. The flat area over the nuclear region (clipped data) indicates that the *z* piezo had reached a maximum travel distance; thus the cell is being imaged in the "constant height" (variable force) mode over this region. (*b*) Original error signal (deflection) data, dominated by noise artifacts. Some larger authentic sample features are apparent, but detail is masked by the noise components. (*c*) FFT analysis of error signal data in *b*, in which noise components are seen as predominantly vertical patterns. The white box indicates the region of passband filtering. (*d*) Resultant error signal data after inverse FFT with passband filtering from *c*. Detail is now revealed, with no masking of image features by the noise. The flat region over the nucleus seen in *a* is not as apparent because the error signal mode data are generated from pixel-to-pixel changes in height, which are minimal when the *z* piezo is at a maximum (or minimum). The noise components were reduced by coupling the sample culture dish to an oil objective on the light microscope. Scale bar = 10 μm. *z* scale = 2 μm.

brief exposures (≤5 s) at 488-nm wavelength excitation before blebbing and lethal effects occurred. The photodynamic effects were not present with excitation of the calcein fluorophore at 529 nm, nor were they present with excitation of EthD-1 at either 488 nm or 529 nm (data not shown).

Because continual epifluorescence observations of XR1 cells in the presence of both fluorophores were precluded by the lethal photodynamic effects of the excited calcein fluorophore, we designed two alternative protocols for the remaining experiments: 1) AFM imaging in cell culture medium only, followed by the 2-fluorophore LIVE/DEAD cell viability assay at fixed time intervals after single- or dual-pass AFM scanning; and 2) AFM imaging of XR1 cells in medium containing EthD-1-1 only, followed by epifluoresence examination. Cells that were examined in ethidium-containing media were also assayed for cell viability at 48 h postscan. The first protocol was advantageous, allowing inspection of neighboring control (non-AFM-scanned) cells, whereas this was not possible during simultaneous AFM imaging and LIVE/DEAD assays, because the field of view in the optical microscope was limited to one or two cells by the 63× objective.

XR1 cells imaged in fluorophore-free media with constant-force contact-mode AFM at 1-Hz fast scan rate and 100 × 100 μm scan size (fast scan rate = 100 $\mu m\ s^{-1}$) were assayed for cell viability and cell death at various postscan times (5–190 min) and disclosed no evidence of cell death (Table 1). We believed that AFM-imaged cells may have survived longer in culture, potentially for days, and thus repeated XR1 cell imaging with the same scan parameters and examined the cells 18–24 h postscan. Cell viability was not significantly affected by AFM imaging when compared to neighboring non-AFM-scanned control cells, or to sham control cells (Table 1).

Because live cells have been imaged by AFM for up to 44 h at scan rates of 3–5 Hz with indications that these cells were still viable at the end of the imaging process (Hoh and Schoenenberger, 1994; Schoenenberger and Hoh, 1994), we modified our protocol to examine the cells at 48 h postimaging. To directly compare our data with those previously reported, contact-mode AFM images were now acquired at both 1-Hz and 5-Hz scan rates. Furthermore, because tapping-mode AFM reduces lateral interactions with the sample (Putman, 1994), we likewise acquired TMAFM images at 1-Hz and 5-Hz scan rates to compare effects on XR1 cell viability between CMAFM and TMAFM.

Fig. 3 presents highpass-filtered height mode data for both contact-mode and tapping-mode AFM images of live XR1 cells in culture and the corresponding cell viability assay results for the 48-h postscan assays. The left column of panels shows BioScope AFM images of live XR1 cells in culture. Cytoskeletal elements (*arrowheads*) were seen in all of the AFM images, although tapping mode in general tended to reveal less of the cytoskeletal details, compared to contact mode under identical imaging parameters; this effect was presumably due to reduced loading forces on the sample in TMAFM. The corresponding LIVE/DEAD *Eukol*ight assays shown in the right columns of the panels indicated that nonspecific esterases were active 48 h after AFM imaging of live XR1 cells in culture, indicating that AFM imaging of live cells does not disrupt this biochemical process. Comparison of cell margins and morphology in AFM images with those revealed during the cell viability assays indicate that XR1 cells continued to undergo changes in shape and size during and after the experimental procedures, providing additional evidence for cell viability. Because EthD-1 was excluded from these AFM-imaged cells (data not shown), we believe that the cell membrane is structurally intact after AFM imaging, and furthermore, that all functions related to cell membrane integrity are also preserved or compensated for during AFM imaging of live cells.

Although these data strongly support cell membrane integrity during AFM imaging of live cells, we repeated the AFM imaging protocols with culture medium containing only the ethidium homodimer-1 fluorophore to investigate the possibility of transient membrane disruptions during imaging. In the eight cells examined (two each for CMAFM 1 Hz or 5 Hz, TMAFM 1 Hz or 5 Hz), EthD-1 fluorescence was not detectable immediately after AFM imaging, and moreover, each imaged cell was viable at 48 h postscan, as evidenced by a positive calcein fluorescence (data not shown). Taken together, these data indicate that single- or dual-pass AFM imaging did not affect XR1 cell viability for a period of up to 48 h postscanning.

TABLE 1 XR1 cell viability assay results

Postimage time	Control	AFM mode and fast scan rate: Contact 1.0 Hz	Contact 5.0 Hz	Tapping mode 1.0 Hz	Tapping mode 5.0 Hz
24 h					
Live	3312*	3	—	10	—
Dead	5	0	—	2	—
48 h					
Live	541	18	18	11	11
Dead	8	0	0	0	0

*Number of cells.

Tip-membrane interactions

Despite the evidence that AFM imaging did not compromise XR1 cell viability in culture, there were indications of acute, transient interactions between the AFM probe and the cell, especially between the stylus tip and the cell membrane. The coaxial nature of the BioScope allowed us to observe the cell with light microscopy during AFM and to acquire real-time video of the probe-cell interactions during the AFM scanning process. The most apparent probe-membrane interactions appeared as pushing and pulling or jiggling of the cell and occurred when the probe was passing over the tallest parts of the cell, namely, while imaging over the nucleus. These findings agree with those of Schoenenberger and Hoh, who reported gross displacement of the nucleus of MDCK cells by the tip during AFM imaging (Schoenenberger and Hoh, 1994). Occasionally an apparent spreading or parting of the membrane was visible, similar to a plow going through a mound of dirt. Interestingly, these same interactions were present in both contact-mode and tapping-mode imaging, although the effects were more pronounced in contact mode for equivalent imaging parameters (i.e., scan size, scan rate, setpoint).

Fig. 4 *a* presents a bright-field videomicroscopy time-lapsed series from an AFM scan during which the cell was torn and subsequently removed from the substrate. Conspicuous probe-membrane interactions occurred as the probe passed over the nucleus, and most notably, portions of the cell membrane actually adhered to the probe. In this AFM scan the cell membrane formed two stringlike attachments to the probe—one to the stylus and the other to the upper leg of the cantilever (Fig. 4, *a4–a8*). These stringlike "trailers" tracked the movement as the probe was scanned in the *x, y* raster pattern and remained attached throughout the scanning process, even as the cell was torn away from the substrate. The trailer adhering to the probe stylus was present from the initiation of the scan and probably attached to the stylus during probe engagement. The trailer adhering to the upper leg of the cantilever attached as the leading edge of the cantilever leg first encountered the nuclear area of the cell (a QuickTime movie of these events is available at the Biophysical Journal WWW and FTP sites).

While the AFM probe scanned over the nuclear region of this same cell, the nucleus and surrounding structures were pushed en masse by the probe during the trace portion of the scan (Fig. 4 *b*). During the retrace, these structures adhered to the probe and were pulled past their original location to a point at which the viscoelastic forces of the cell were greater than the attractive forces of the probe. At this point, the nuclear structures recoiled from the probe and came to rest at a position slightly closer to the undamaged side of the cell. The resultant AFM image indicates that the nuclear portion of this XR1 cell had been completely removed, and yet the cytoplasmic regions appear to remain intact and adherent to the substrate (Fig. 5 *k*). An FM 1-43 assay of the probe from this scan reveals that the probe stylus and the entire expanse of the cantilever were coated with membrane components from this cell (Fig. 5 *l*).

Noticeable probe-cell interactions in bright-field microscopy generally correlated with less resolved and lower quality AFM images, and thus we

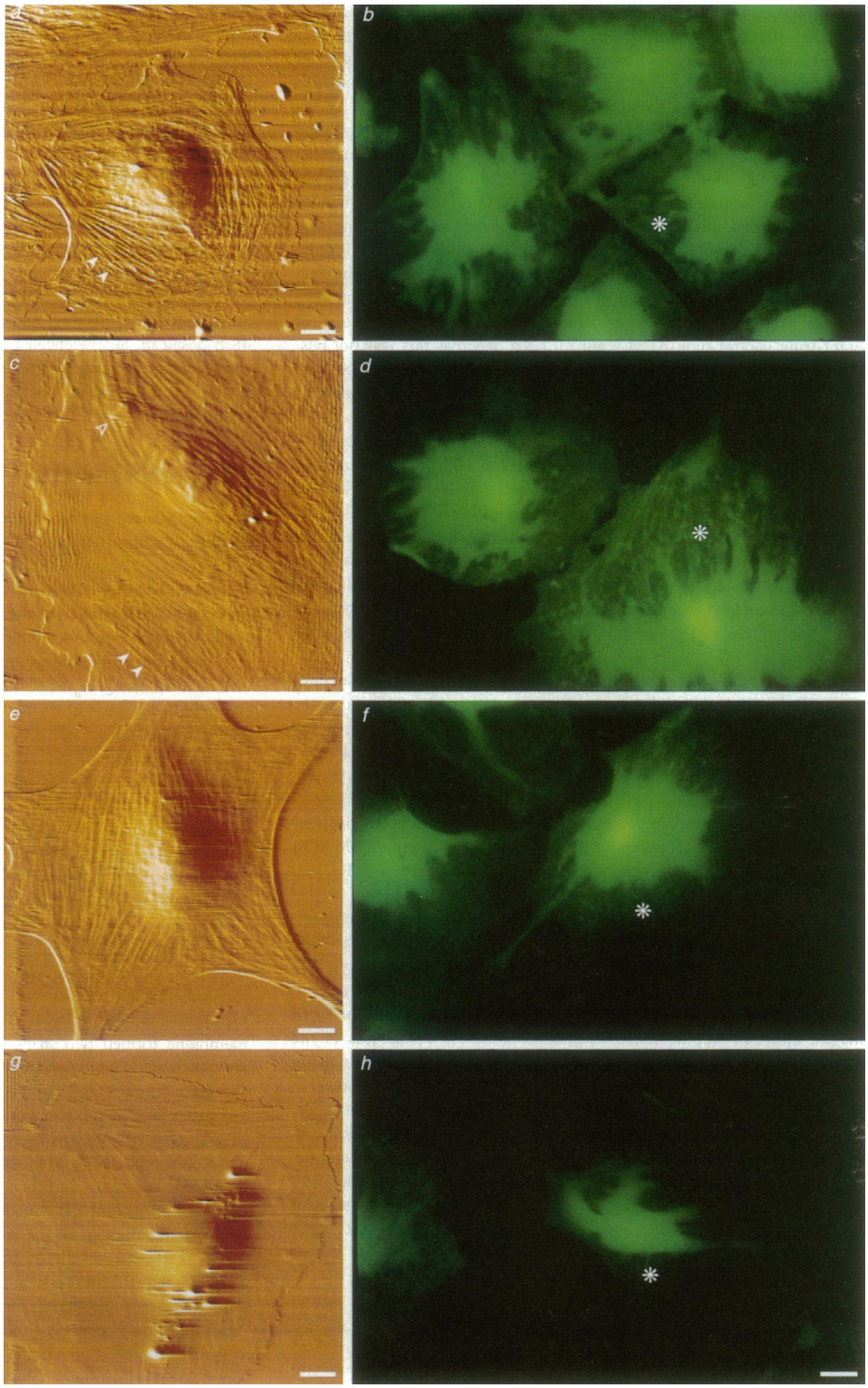

FIGURE 3 AFM images and cell viability assay fluorescence photomicrographs of live XR1 cells in culture. Image pairs represent AFM images (*left*) and corresponding cell viability assays (*right*). All AFM images are highpass-filtered height. Fluorescence photomicrographs were taken 48 h post-AFM scanning and show live cell assay (calcein) results. The asterisk indicates the cell corresponding to the AFM image. The respective dead cell assays were all negative and thus are not shown. (*a*) Contact mode AFM image, 1.0-Hz fast scan rate. Prominent cytoskeletal elements (*closed arrowheads*) are revealed by contact mode imaging. Contacts with neighboring cells are seen in the left half of the image. These neighboring cells were also imaged by AFM and are seen in the corresponding live cell assay photomicrograph. (*c*) TappingMode AFM image, 1.0-Hz fast scan rate. The cytoskeletal elements (*closed arrowheads*) are not as prominent, compared to the contact mode image acquired at 1.0 Hz, and the nucleus is not as tall. This cell has a characteristic elongated, spread-out appearance and may represent a cell that is about to undergo mitosis; the open arrowhead indicates a structure that is conceivably a centriole. (*e*) Contact-mode AFM image, 5.0-Hz fast scan rate. Cytoskeletal elements are not as prominent, compared to the contact mode image acquired at 1.0 Hz, but the cell margins are more prominent. (*g*) Tapping-mode AFM image, 5.0-Hz scan rate. The cytoskeletal elements are least visible with these parameters, but there are conspicuous probe-sample interaction artifacts over the nuclear region of the cell. These artifacts appear as peaked structures that are oriented in the fast scan trace direction. Scales: AFM, bar = 10 μm, z = 2 μm; photomicrographs, bar = 25 μm.

propose that AFM image quality can provide an initial indicator for the magnitude of probe-cell interaction, much as the AFM image quality of DNA samples serves as an indicator of probe-sample interactions (Vesenka et al., 1993).

Because AFM probes occasionally acquired visible membrane "trailers" and because the interactions between the Si_3N_4 probe stylus and the cell membrane have not been well documented, we wondered whether there was measurable membrane accumulation on the probe during AFM imaging. To this end we used FM 1-43, a fluorophore that intercalates between the hydrophobic tails of phospholipids and that has been used to monitor vesicle cycling in neurons (Betz and Bewick, 1992; Betz et al., 1992a,b; Meffert et al., 1994), to examine AFM probes from the cell-scanning experiments and report whether membrane accumulated on the probes. Fig. 5 is a gallery of composite AFM probe images (in which the FM 1-43

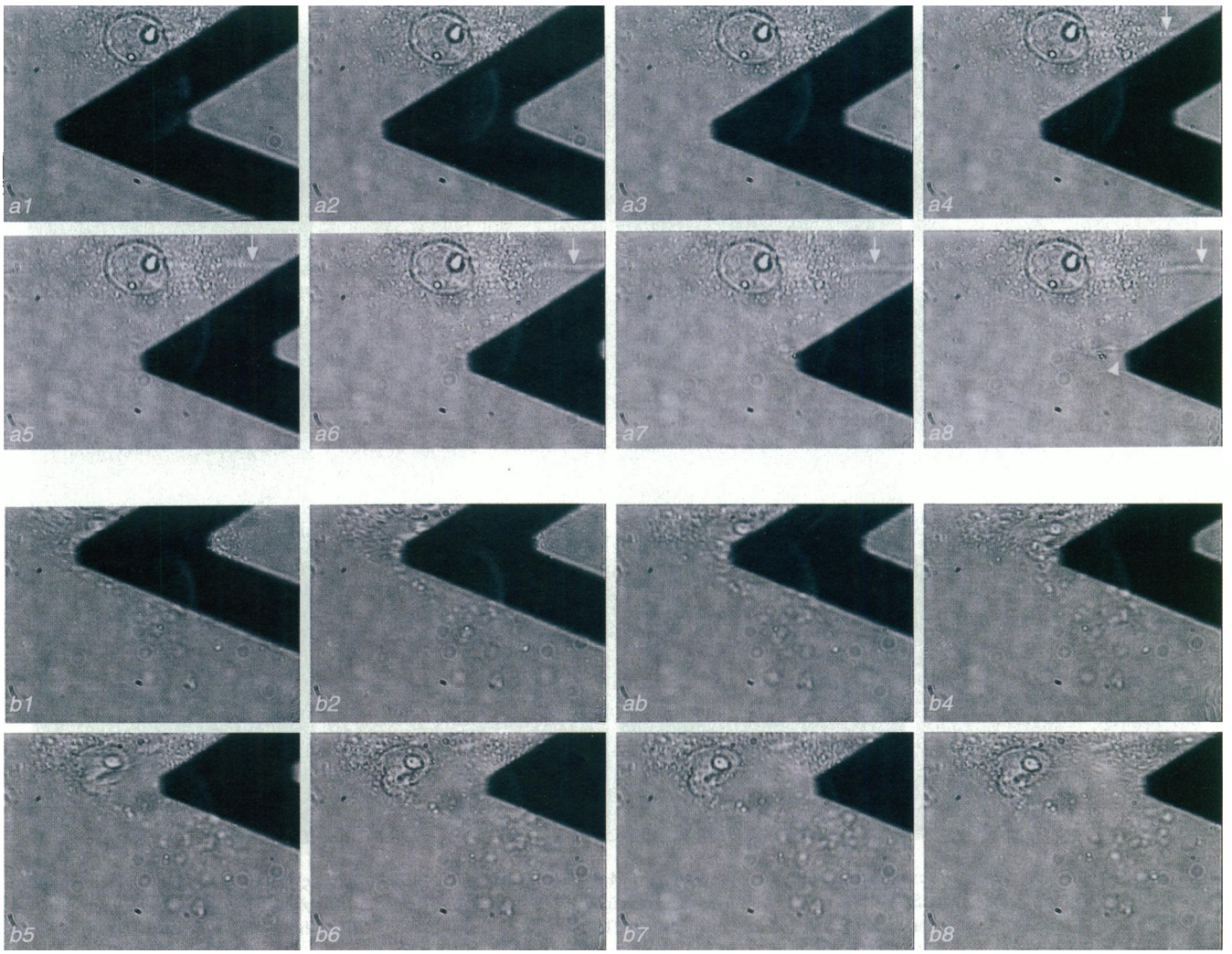

FIGURE 4 AFM probe-cell membrane interactions and membrane attachment to AFM probe. Each panel in these time-lapsed series is an individual frame capture (1/15 s interval between frames, every other frame from 30 fps) from a videomicrograph of an AFM imaging session. Contrast was enhanced globally in each frame to reveal detail. (*a1–a8*) Attachment of cell membrane to AFM probe during AFM imaging. AFM parameters: tapping mode, 5.0-Hz fast scan rate, slow scan direction = up. The nucleus of this XR1 glial cell is in the upper center of the field, delimited by a darker margin. As the probe scanned from the left to right (retrace), a stringlike portion of cell membrane attached to the upper cantilever leg (*down arrow*). As the probe moved away from the nucleus, this membranous attachment became more well defined, and did not release from the probe. In frame *a8* a less well-defined attachment of membrane to the probe stylus becomes apparent (*arrowhead*). This attachment also tracked the probe movement and did not release from the probe stylus. See Fig. 5 *k* for the AFM image of this XR1 cell. (*b1–b8*) Removal of nuclear area of an XR1 cell during AFM imaging. Panels *b1–b8* are a continuation of the time-lapsed series as the AFM probe scans over the nuclear region of the cell. The nucleus is located in the upper portion of each frame, but in *b1* the nucleus has been displaced to the left of the frame (compare to *a1*). The nucleus tracked the probe until the elastic recoil force of the nucleus was greater than the attractive force of the probe, and the nucleus released and recoiled from the probe (*b5*). As the probe moved away from the recoiled nucleus, a thin membranous attachment to the probe became evident (*arrow*). The resulting AFM image is shown in Fig. 5 *k*. The nuclear area of this cell has been completely removed, yet the surrounding cytoplasmic areas remained intact. The upper half of the scan is less resolved, presumably because of an increased effective stylus radius as membrane accumulated on the probe. A heavy accumulation of membrane on the probe is revealed by FM 1-43 staining and confocal microscopy (Fig. 5 *l*).

fluorescence image is overlaid on a reflected image; see Materials and Methods) and the corresponding AFM image of the cell. In both contact-mode and tapping-mode AFM images, membrane accumulated on the stylus, sometimes to a qualitatively greater extent on the stylus face leading the slow scan direction (indicated by *arrows*). Membrane accumulation on the probes used in tapping-mode imaging occurred generally in more punctate patterns (*c,d* and *g,h*), correlating with reduced lateral interaction between the probe and the cell membrane, whereas membrane accumulation on probes used in contact mode imaging often showed larger patchy patterns (*a,b* and *e,f*). Membrane accumulation on probes occurred even during optimal scanning conditions (i.e., high resolution obtained with minimal loading forces and no apparent visible probe-cell interactions), as Fig. 5 *j* shows. A prominent membrane accumulation occurred on the lower leg of the cantilever, with a thin extension of membrane connecting to the patchy deposit of membrane on the stylus, and yet the AFM image does not reveal flagrant damage to the cell. There was no correlation in the data between cell height (1.5–4.5 μm) and the amount or pattern of lipid accumulation, or between scan parameters or scan mode and lipid accumulation.

For control data in the FM 1-43 assays, new AFM probes were scanned over either uncoated glass coverslips or cell-free ECL-coated glass coverslips, or repeated "force curves" were taken over cytoplasmic and nuclear areas of live XR1 cells in culture. FM 1-43 fluorescence assays on all

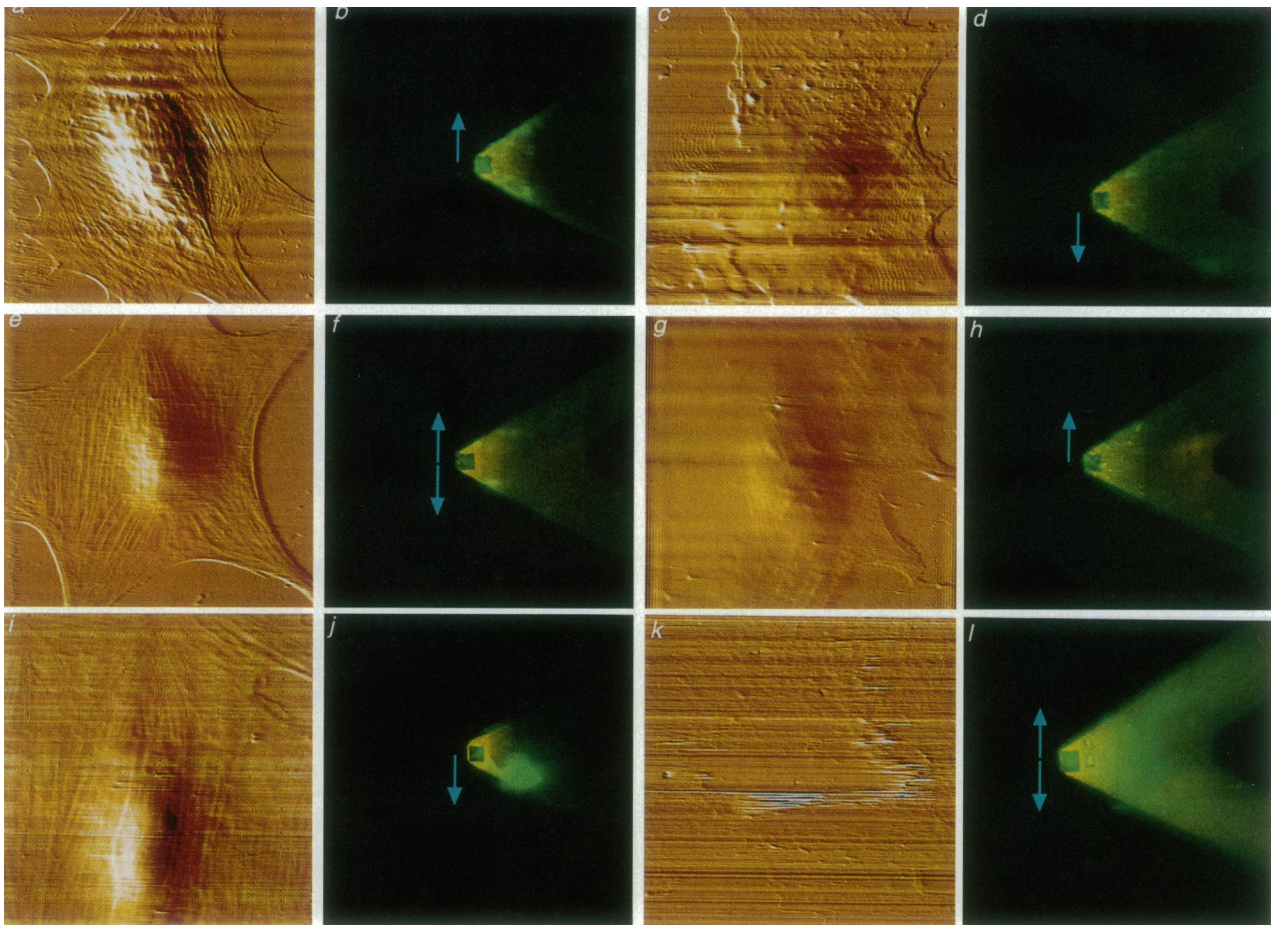

FIGURE 5 FM 1-43 fluorescence reveals membrane components on AFM probes used in live cell scans. Image pairs are AFM (*left*) and composite confocal laser scanning microscopy (CSLM) FM 1-43 fluorescence assays (*right*). (*a,b*) AFM, Contact mode, 1.0-Hz fast scan rate, slow scan direction = up; prominent cytoskeleton, tall nuclear area, distinct cell margins. CSLM, The probe stylus was fully covered with membrane components, as were the edges of the cantilever legs. (*c,d*) AFM, Tapping mode, 1.0-Hz fast scan rate, slow scan direction = down; this cell has the characteristic appearance of a cell that may be entering mitosis—elongated, spread-out cytoplasm, shorter nuclear height. CSLM, Membrane components accumulated in a more punctate pattern, compared to contact mode. (*e,f*) AFM, Contact mode, 5.0-Hz fast scan rate, slow scan direction = up + down; cytoskeletal elements are less prominent than at a 1.0-Hz scan rate. CSLM, Membrane accumulations are intermediate, between patchy and punctate. (*g,h*) AFM, Tapping mode, 5.0-Hz fast scan rate, slow scan direction = up; few cytoskeletal elements are visible, and the image is generally "soft," because it was imaged with the minimum applied vertical force needed to form a resolved image. CSLM, Membrane accumulation is still punctate, but approaching a patchy pattern; significant accumulations occurred along the cantilever legs, probably because of tall cell nuclear area. (*i,j*) AFM, Contact mode, 10-Hz fast scan rate, slow scan direction = down; this is a large cell, filling the entire image field, cytoskeletal elements are not as conspicuous as in *a*, even with the same imaging parameters; the original AFM image was filtered in Fourier space to remove a strong noise component—the sample vibrations causing the noise may have been related to the considerable probe-membrane interactions. CSLM, There is a large accumulation of membrane along the leading edge of the cantilever; this deposit is attached to the patchy accumulation on the stylus by a strand of membrane. (*k,l*) AFM, Tapping mode, 5.0-Hz fast scan rate, slow scan direction = up; the nuclear region of this cell was excised by the AFM probe during imaging (see Fig. 4), but the cytoplasmic area remained attached to the substrate. CSLM, The entire probe (stylus and cantilever) is covered with membrane, confirming the substantial interaction between the probe and the cell membrane. Scale bars = 10 μm.

probes from these controls were negative (data not shown). The control data suggest that either the brief dwell time or the vertical interaction between the probe and cell membrane during force curves may not be sufficient to produce membrane transfer to the probe. Combining these findings with those of reduced membrane accumulations on the probe during TMAFM, we speculate that lateral interactions between the probe and cell membrane are the major determinant of membrane transfer to AFM probe tips during imaging of live cells.

CONCLUSION

With the LIVE/DEAD *Euko*Light assay, which affords rapid and specific determination of biochemical cell viability and physical and physiological membrane integrity, we provide evidence that single- and dual-pass scanning in both contact-mode and tapping-mode AFM imaging of live XR1 cells is not deleterious to cell viability or cell membrane integrity for up to 48 h postscanning. An extension of these results will be to perform continuous AFM scanning for varied durations and then examine cell viability to determine the limitations, if any, upon AFM scanning of live cells.

Although the results from the cell viability assays are encouraging for the future of biological AFM of live cells, it should be noted that there are substantial interactions

between the AFM probe and the cell membrane that lead to membrane accumulation on the probe tip, even during "ideal" imaging conditions. In some cases the membrane accumulation appeared to slightly favor the slow scan direction face of the pyramidal stylus, although our results are strictly qualitative and require further corroboration. Identification of the membrane components in the probe accumulations could provide further insight into the "penetration" versus "draping" models, in that phospholipid composition often varies between the membrane inner and outer leaflets. Furthermore, it is important to determine whether the membrane accumulations on the probe are due to adsorption or to other phenomena.

Our evidence for the prolonged viability of XR1 cells in culture after AFM imaging further supports the application of AFM to the study of live cells and specimens, but also points out limitations of current methods. The controllable, precise nature of the AFM should facilitate the selective introduction of materials into living cells, for example, controlled injection of transforming vectors directly over the nuclear area of a eukaryotic cell. These same AFM characteristics, combined with the directed deposition or accumulation of specific materials on an AFM probe tip, may lead to the controlled rearrangement of membrane components, such as receptors and channels, or may facilitate directed insertion of exogenous components into the membrane, circumventing host cell expression of the constituent.

Finally, establishing the viability of cells in culture for extended periods after AFM imaging provides the foundation for extended AFM time course studies of live samples, examples of which include developmental processes, such as neurite targeting and outgrowth; exocytotic and endocytotic processes, such as synaptic vesicle fusion, or receptor-mediated endocytosis (RME); and localization and mapping of receptors and receptor clustering in vitro.

We thank Don Sakaguchi and Tim Folsom for providing and supporting the XR1 cell line, and Mike Haynes for photographic and image assistance.

SSS was supported by a National Science Foundation Signal Transduction Training grant. This paper was journal paper no. J-17477 of the Iowa Agriculture and Home Economics Experiment Station, Ames, IA, project no. 3064, and was supported by the Hatch Act and State of Iowa Funds.

REFERENCES

Barbee, K. A., P. F. Davies, and R. Lal. 1994. Shear stress-induced reorganization of the surface topography of living endothelial cells imaged by atomic force microscopy. *Circ. Res.* 74:163–171.

Barbee, K. A., T. Mundel, R. Lal, and P. F. Davies. 1995. Distribution of shear stress on the surface of aligned and non-aligned endothelial monolayers. *Adv. Bioeng.* 28:349–350.

Beckmann, M., H. A. Kolb, and F. Lang. 1994. Atomic force microscopy of peritoneal macrophages after particle phagocytosis. *J. Membr. Biol.* 140:197–204.

Betz, W. J., and G. S. Bewick. 1992. Optical analysis of synaptic vesicle recycling at the frog neuromuscular junction. *Science.* 200:200–203.

Betz, W. J., G. S. Bewick, and R. M. A. P. Ridge. 1992a. Intracellular movements of fluorescently labeled synaptic vesicle in frog motor nerve terminals during nerve stimulation. *Neuron.* 9:805–813.

Betz, W. J., F. Mao, and G. S. Bewick. 1992b. Activity-dependent fluorescent staining and destaining of living vertebrate motor nerve terminals. *J. Neurosci.* 12:363–375.

Binnig, G., C. F. Quate, and C. Gerber. 1986. Atomic force microscope. *Phys. Rev. Lett.* 56:930–933.

Bonfiglio, A., M. T. Parodi, and G. P. Tonini. 1995. Subcellular details of early events of differentiation induced by retinoic acid in human neuroblastoma cells detected by atomic force microscope. *Exp. Cell Res.* 216:73–79.

Braunstein, D., and A. Spudich. 1994. Structure and activation dynamics of RBL-2H3 cells observed with scanning force microscopy. *Biophys. J.* 66:1717–1725.

Chang, L., T. Kious, M. Yorgancioglu, D. Keller, and J. Pfeiffer. 1993. Cytoskeleton of living, unstained cells imaged by scanning force microscopy. *Biophys. J.* 64:1282–1286.

D'Costa, N. P., and J. H. Hoh. 1995. Calibration of optical lever sensitivity for atomic force microscopy. *Rev. Sci. Instrum.* 66:1–2.

Fritz, M., M. Radmacher, and H. E. Gaub. 1994. Granula motion and membrane spreading during activation of human platelets imaged by atomic force microscopy. *Biophys. J.* 66:1328–1334.

Häberle, W., J. K. Hörber, F. Ohnesorge, D. P. Smith, and G. Binnig. 1992. In situ investigations of single living cells infected by viruses. *Ultramicroscopy.* 42–44:1161–1167.

Haydon, P. G., R. Lartius, V. Parpura, and S. P. Marchese Ragona. 1996. Membrane deformation of living glial cells using atomic force microscopy. *J. Microsc.* 182:114–120.

Henderson, E., P. G. Haydon, and D. S. Sakaguchi. 1992. Actin filament dynamics in living glial cells imaged by atomic force microscopy. *Science.* 257:1944–1946.

Hoh, J. H., and C. A. Schoenenberger. 1994. Surface morphology and mechanical properties of MDCK monolayers by atomic force microscopy. *J. Cell Sci.* 107:1105–1114.

Hörber, J. K., W. Häberle, F. Ohnesorge, G. Binnig, H. G. Liebich, C. P. Czerny, H. Mahnel, and A. Mayr. 1992. Investigation of living cells in the nanometer regime with the scanning force microscope. *Scanning Microsc.* 6:919–929 (discussion 929–930).

Hörper, R., T. Gesang, W. Possart, O.-D. Hennemann, and S. Boseck. 1995. Imaging elastic sample properties with an atomic force microscope operating in the tapping mode. *Ultramicroscopy.* 60:17–24.

Kasas, S., V. Gotzos, and M. R. Celio. 1993. Observation of living cells using the atomic force microscope. *Biophys. J.* 64:539–544.

Lal, R., B. Drake, D. Blumberg, D. R. Saner, P. K. Hansma, and S. C. Feinstein. 1995. Imaging real-time neurite outgrowth and cytoskeletal reorganization with an atomic force microscope. *Am. J. Physiol.* 269: C275–C285.

Le Grimellec, C., E. Lesniewska, C. Cachia, J. P. Schreiber, F. De Fornel, and J. P. Goudonnet. 1994. Imaging of the membrane surface of MDCK cells by atomic force microscopy. *Biophys. J.* 67:36–41.

Meffert, M. K., B. A. Premack, and H. Schulman. 1994. Nitric oxide stimulates Ca^{2+}-independent synaptic vesicle release. *Neuron.* 12: 1235–1244.

Oberleithner, H., G. Giebisch, and J. Geibel. 1993. Imaging the lamellipodium of migrating epithelial cells in vivo by atomic force microscopy. *Pflügers Arch.* 425:506–510.

Oberleithner, H., A. Schwab, W. Wang, G. Giebisch, F. Hume, and J. Geibel. 1994. Living renal epithelial cells imaged by atomic force microscopy. *Nephron.* 66:8–13.

Parpura, V., P. G. Haydon, D. S. Sakaguchi, and E. Henderson. 1993. Atomic force microscopy and manipulation of living glial cells. *J. Vac. Sci. Technol. A.* 11:773–775.

Putman, C. A. J. 1994. Tapping atomic force microscopy in liquids. *Appl. Phys. Lett.* 64:2454–2456.

Putman, C. A., K. O. van der Werf, B. G. de Grooth, N. F. van Hulst, and J. Greve. 1994. Viscoelasticity of living cells allows high resolution imaging by tapping mode atomic force microscopy. *Biophys. J.* 67: 1749–1753.

Putman, C. A. J., K. van der Werk, B. G. de Grooth, N. F. van Hulst, J. Greve, and P. K. Hansma. 1992. A new imaging mode in atomic force microscopy based on the error signal. *SPIE.* 1639:198–204.

Radmacher, M., M. Fritz, and P. K. Hansma. 1995. Imaging soft samples with the atomic force microscope: gelatin in water and propanol. *Biophys. J.* 69:264–270.

Raedler, J., M. Radmacher, and H. E. Gaub. 1995. Velocity-dependent forces in atomic force microscopy imaging of lipid films. *Langmuir.* 10:3111–3115.

Ricci, D., and M. Grattarola. 1994. Scanning force microscopy on live cultured cells: imaging and force-versus-distance investigations. *J. Microsc.* 176:254–261.

Sakaguchi, D. S., and E. Henderson. 1993. Isolation and characterization of glial cell lines from Xenopus neuroepithelium and retinal pigment epithelium. *Neuroprotocols.* 3:249–259.

Sakaguchi, D. S., J. F. Moeller, C. R. Coffman, N. Gallenson, and W. A. Harris. 1989. Growth cone interactions with a glial cell line from embryonic Xenopus retina. *Dev. Biol.* 134:158–174.

Schneider, S. W., K. C. Sritharan, J. P. Geible, H. Oberleithner, and B. P. Jena. 1997. Surface dynamics in living acinar cells imaged by atomic force microscopy: identification of plasma membrane structures involved in exocytosis. *Proc. Natl. Acad. Sci. USA.* 94:316–321.

Schoenenberger, C. A., and J. H. Hoh. 1994. Slow cellular dynamics in MDCK and R5 cells monitored by time-lapse atomic force microscopy. *Biophys. J.* 67:929–936.

Schwab, A., K. Gabriel, F. Finsterwalder, G. Folprecht, R. Greger, A. Kramer, and H. Oberleithner. 1995. Polarized ion transport during migration of transformed Madin-Darby canine kidney cells. *Pflügers Arch.* 430:802–807.

Shroff, S. G., D. R. Saner, and R. Lal. 1995. Dynamic micromechanical properties of cultured rat atrial myocytes measured by atomic force microscopy. *Am. J. Physiol.* 269:C286–C292.

Spudich, A., and D. Braunstein. 1995. Large secretory structures at the cell surface imaged with scanning force microscopy. *Proc. Natl. Acad. Sci. USA.* 92:6976–6980.

Tao, N. J., S. M. Lindsay, and S. Lees. 1992. Measuring the microelastic properties of biological material. *Biophys. J.* 63:1165–1169.

Vesenka, J., S. Manne, G. Yang, C. J. Bustamante, and E. Henderson. 1993. Humidity effects on atomic force microscopy of gold-labeled DNA on mica. *Scanning Microsc.* 7:781–788.

Vesenka, J., C. Mosher, S. Schaus, L. Ambrosio, and E. Henderson. 1995. Combining optical and atomic force microscopy for life sciences research. *Biotechniques.* 19:240–248, 849, 852–243.